

Freezing of spin correlated nanoclusters in a geometrically frustrated magnet

W. Ratcliff II,¹ S.-H. Lee,^{2,3} C. Broholm,^{2,4} S.-W. Cheong,¹ and Q. Huang²¹Department of Physics and Astronomy, Rutgers University, Piscataway, New Jersey 08854²NIST Center for Neutron Research, National Institute of Standards and Technology, Gaithersburg, Maryland 20899³Department of Physics, University of Maryland, College Park, Maryland 20742⁴Department of Physics and Astronomy, The Johns Hopkins University, Baltimore, Maryland 21218

(Received 10 January 2002; published 13 June 2002)

The effects of disorder on the geometrically frustrated magnet ZnCr_2O_4 are examined through magnetic susceptibility and inelastic neutron-scattering measurements on $\text{Zn}_{1-x}\text{Cd}_x\text{Cr}_2\text{O}_4$. 3% Cd doping destroys the Néel order of the parent compound, replacing it with a frozen phase of spin-correlated nanoclusters. The local spin structure of these nanoclusters endures through the paramagnetic, spin-glass, and Néel phases of the material.

DOI: 10.1103/PhysRevB.65.220406

PACS number(s): 75.50.Lk, 75.40.Gb, 75.50.Ee, 76.50.+g

Like low dimensionality, competing interactions and weak connectivity can suppress long-range order in interacting spin systems.¹ Classifying the alternative low-temperature phases in such “geometrically frustrated” magnets is an active area of research with possible ramifications in many areas of science.² One of the most common low-temperature phases is a quasistatic or “frozen” short-range ordered state. Such disordered phases have been found in seemingly pure crystalline systems leading to speculations that they represent a disorder-free spin glass.³ However, it is notoriously difficult to prove the absence of relevant disorder in real materials. $\text{Y}_2\text{Mo}_2\text{O}_7$ was, for example, considered a prime example of a disorder free spin glass⁴ until extended x-ray-absorption fine structure experiments⁵ recently revealed significant structural disorder with a potential impact on the spin Hamiltonian.^{7,6}

Rather than pursuing an elusive clean limit in materials where it may be unattainable, we have studied a geometrically frustrated spinel antiferromagnet, ZnCr_2O_4 where Néel ordered samples are available.⁸ We can then move from a Néel ordered phase back to a disordered phase in a controlled manner by adding chemical dopants. Our susceptibility and neutron-scattering experiments on these samples reveal extreme sensitivity to quenched disorder. In particular, 3% substitution of cadmium for zinc completely suppresses Néel order in $\text{Zn}_{1-x}\text{Cd}_x\text{Cr}_2\text{O}_4$, replacing it by hysteretic short-range order. We also show that the local structure of the frozen state in $\text{Zn}_{0.95}\text{Cd}_{0.05}\text{Cr}_2\text{O}_4$ closely resembles that of the cooperative paramagnetic phase. Our interpretation is that bond disorder yields strong pinning centers for preformed composite spin degrees of freedom in geometrically frustrated magnets and that such pinning effects are the likely cause of spin-glass-like phases in these systems.

Polycrystalline specimens were prepared by solid-state reaction between stoichiometric amounts of Cr_2O_3 , ZnO , and CdO in air. For the neutron-scattering experiments, ^{114}CdO was used due to the high nuclear absorption cross section of ^{112}CdO . All samples were adjudged single phase from measurements performed on a Rigaku x-ray diffractometer. Rietveld analysis of neutron powder diffraction data from our $\text{Zn}_{0.95}\text{Cd}_{0.05}\text{Cr}_2\text{O}_4$ sample showed that it is a single phase

spinel with space group $Fd\bar{3}m$, and lattice parameter $a = 8.3321(2)$ Å at $T = 15$ K. Elastic and inelastic neutron-scattering measurements were performed at NIST on the cold neutron triple-axis spectrometer SPINS using a configuration described elsewhere.⁸ Magnetic susceptibility was measured in a dc field of 100 Oe using a Quantum Design superconducting quantum interference device magnetometer.

Figures 1(a) and 1(b) show susceptibility data for polycrystalline $\text{Zn}_{1-x}\text{Cd}_x\text{Cr}_2\text{O}_4$ samples. A reduction in susceptibility by approximately 1/3 signals the phase transition to

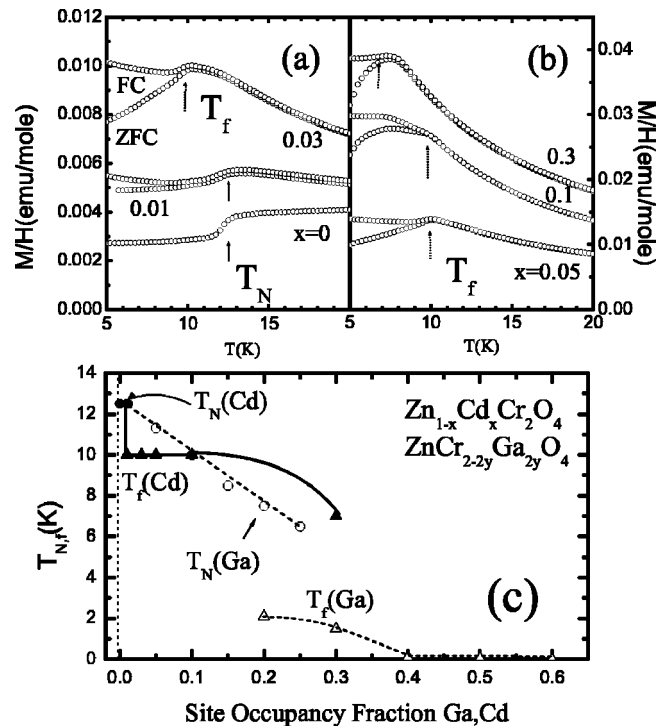


FIG. 1. (a), (b) Bulk susceptibility data measured in a dc field of 100 Oe on ceramic samples of $\text{Zn}_{1-x}\text{Cd}_x\text{Cr}_2\text{O}_4$. (c) Phase diagram of the $\text{Zn}_{1-x}\text{Cd}_x\text{Cr}_2\text{O}_4$ and $\text{ZnCr}_{2-2y}\text{Ga}_y\text{O}_4$ series. Solid lines and symbols are for Cd doping while dashed lines and open symbols are for Ga doping. The data for $\text{ZnCr}_{2-2y}\text{Ga}_y\text{O}_4$ are reproduced from Ref. 9.

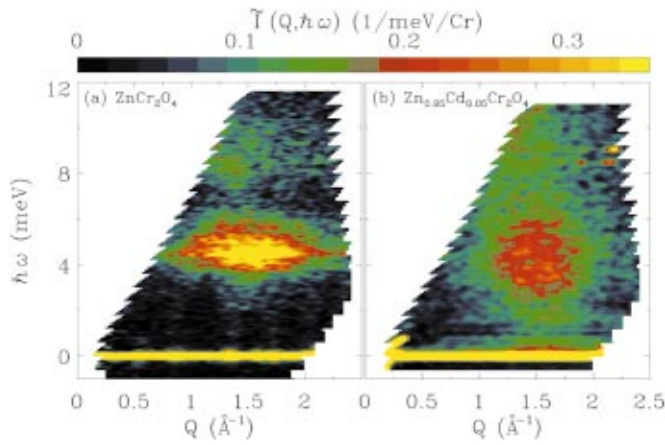


FIG. 2. (Color) Color contour maps of the magnetic neutron-scattering intensity versus wave vector and energy transfer: $\tilde{\Gamma}(Q, \omega)$, at 1.5 K obtained from (a) ZnCr_2O_4 and (b) $\text{Zn}_{0.95}\text{Cd}_{0.05}\text{Cr}_2\text{O}_4$.

long-range Néel order for $x=0$. While there is no appreciable difference between zero-field-cooled (ZFC) and field-cooled (FC) data for the pure sample, just 1% Cd substitution for Zn yields history dependence of the magnetization, which indicates that Néel order is replaced by a spin-glass-like state at low temperatures. From anomalies in $\chi(\text{FC}) - \chi(\text{ZFC})$ for $\text{Zn}_{1-x}\text{Cd}_x\text{Cr}_2\text{O}_4$ samples with $0 \leq x \leq 0.3$, we derived the phase boundary between the paramagnetic and spin-glass-like phases, which is reported in Fig. 1(c). Despite the identical valence of Cd and Zn in $\text{Zn}_{1-x}\text{Cd}_x\text{Cr}_2\text{O}_4$, the 1.3 times greater ionic radius of Cd^{2+} yields lattice strain around defects that in turn could lead to changes in exchange interactions, single-ion anisotropy, and elastic properties. A different type of disorder can be achieved by substituting nonmagnetic gallium for magnetic chromium atoms. Figure 1(c) shows a remarkable contrast between the effects of bond disorder and magnetic dilution. Néel order survives 25% nonmagnetic dilution with a spin-glass-like phase emerging at higher dilution.

For further information about spin correlations in doped samples, we turn to magnetic neutron scattering. Focusing first on low-temperature properties, Fig. 2 shows color contour maps of neutron-scattering intensity $\tilde{\Gamma}(Q, \omega)$ obtained at 1.5 K from the Néel phase of ZnCr_2O_4 and from the spin-glass-like phase of $\text{Zn}_{0.95}\text{Cd}_{0.05}\text{Cr}_2\text{O}_4$. In pure ZnCr_2O_4 , most of the low-energy spectral weight is concentrated in a local resonance centered at $\hbar\omega = 4.5 \text{ meV} \approx |J| \gg k_B T_f$ and with a full width at half maximum (FWHM) of 0.8 meV. Below the resonance, there are spin waves with an energy gap $\leq 0.5 \text{ meV}$.⁸ Not visible in Fig. 2(a), are magnetic Bragg peaks that contribute to the elastic scattering and bear witness to long-range magnetic order. A finite-energy maximum in the scattering intensity clearly survives for $\text{Zn}_{0.95}\text{Cd}_{0.05}\text{Cr}_2\text{O}_4$. However the FWHM has increased by a factor of five, to 4 meV. There is also quasielastic scattering reflecting the static correlations that are apparent from the hysteretic magnetization data. At all energies the magnetic

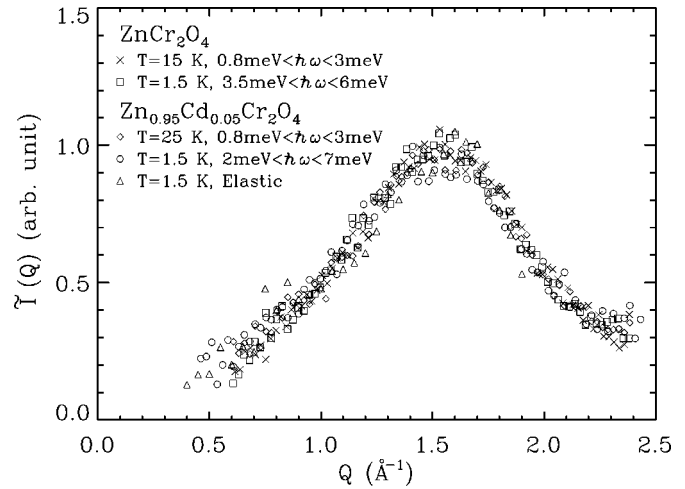


FIG. 3. Q dependence of magnetic neutron-scattering from $\text{Zn}_{1-x}\text{Cd}_x\text{Cr}_2\text{O}_4$ for various values of temperature and doping that are indicated in the figure. Different data sets have been scaled to overlay as best possible.

scattering cross section for $\text{Zn}_{1-x}\text{Cd}_x\text{Cr}_2\text{O}_4$ has a broad maximum close to $Q = 1.5 \text{ \AA}^{-1}$ indicating short-range anti-ferromagnetic correlations.

To examine the latter aspect of the data more carefully, Figure 3 shows the wave-vector dependence of the magnetic scattering cross section for pure and Cd-doped ZnCr_2O_4 integrated over various energy ranges. The figure reveals that the Q -dependence of all the magnetic scattering observed in $\text{Zn}_{0.95}\text{Cd}_{0.05}\text{Cr}_2\text{O}_4$ for $\hbar\omega < 7 \text{ meV}$ follows a “universal” curve. We also find the same wave-vector dependence for inelastic neutron scattering in the paramagnetic phase of the pure sample and for the 4.5 meV resonance in the long-range ordered phase. The persistence of a specific wave-vector dependence over a wide range of conditions invokes the notion of a form factor in the scattering cross section. A conventional magnetic form factor arises from the finite spatial distribution of the atomic spin density, which in turn is determined by intra-atomic Coulomb interactions. While interatomic exchange interactions induce correlations between the atomic spin on different atoms, they are too weak to change the intra-atomic spin-density distribution. Consequently, the neutron-scattering cross section has an overall form factor that remains largely the same for all materials with a given magnetic ion. The robust nature of the Q -dependence of the magnetic scattering cross section for $\text{Zn}_{1-x}\text{Cd}_x\text{Cr}_2\text{O}_4$ suggests that in this material, interatomic interactions establish rigid nanoscale spin clusters. The corresponding cluster form factor affects the magnetic neutron-scattering cross section throughout the wide range of conditions that leave spin correlations within nanoclusters intact. From the fact that the cross section in Fig. 3 appears to vanish as Q goes to zero we infer that the clusters carry no net magnetization and from the half width at half maximum of the peak, $\kappa = 1.1a^*$, we infer a cluster size of order the nearest-neighbor Chromium spacing.

We now examine the effects of disorder on the nanocluster spin-fluctuation spectrum. Figure 4 shows the frequency dependence of the imaginary part of the spin susceptibility

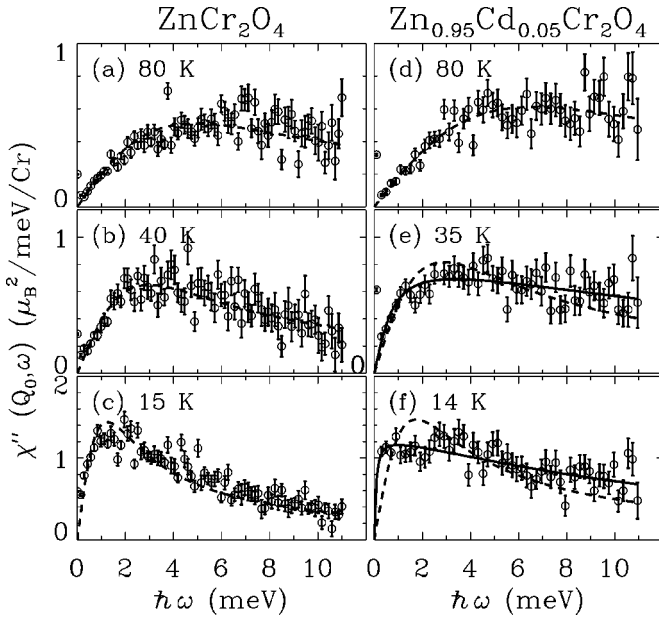


FIG. 4. The frequency dependence of the imaginary part of the spin susceptibility, $\chi''(Q_0, \omega)$ for $Q_0 = 1.5 \text{ \AA}^{-1}$ as derived from magnetic neutron-scattering data via the fluctuation dissipation theorem. (a)–(c) show data for pure ZnCr_2O_4 while (d)–(f) are for $\text{Zn}_{0.95}\text{Cd}_{0.05}\text{Cr}_2\text{O}_4$. Dashed lines are fits to a Lorentzian spectrum with a single characteristic relaxation rate, while the solid lines are fits to Eq. (1).

for ZnCr_2O_4 and $\text{Zn}_{0.95}\text{Cd}_{0.05}\text{Cr}_2\text{O}_4$ at three different temperatures in the paramagnetic phase. The data were derived from magnetic neutron scattering at $Q = 1.5 \text{ \AA}^{-1}$ via the fluctuation dissipation theorem.¹⁰ At $T = 80 \text{ K}$, $\chi''(Q, \omega)$ is not strongly affected by disorder. A Lorentzian spectral function $\chi''(Q, \omega) = \chi_Q \Gamma_Q \omega / (\omega^2 + \Gamma_Q^2)$ can account for data

from both samples and the derived relaxation rates $\Gamma_Q = 5.0(4) \text{ meV}$ and $6.6(4) \text{ meV}$ for the pure and doped samples are close. Cooling not only shifts spectral weight towards lower energies, but for the doped sample there are also qualitative changes in the spectrum. While the pure sample at $T = 40 \text{ K}$ has a Lorentzian spectrum with a characteristic relaxation rate $\Gamma_Q = 3.0(2) \text{ meV}$, the spectrum for the doped sample is not as sharply peaked. The anomalously flat spectrum can be associated with a broadened relaxation rate distribution.^{11,12} To extract limits for this distribution, we used the following phenomenological response function:

$$\chi''(Q, \omega) = \int d\Gamma \rho(\Gamma) \frac{\chi_Q \Gamma \omega}{\Gamma^2 + \omega^2} = \frac{\chi_Q}{\ln(\Gamma_2/\Gamma_1)} \left[\tan^{-1}\left(\frac{\omega}{\Gamma_1}\right) - \tan^{-1}\left(\frac{\omega}{\Gamma_2}\right) \right]. \quad (1)$$

Here $\Gamma_{1(2)}$ are the low- (high-) frequency cutoff for a relaxation rate distribution $\rho(\Gamma) \propto 1/\Gamma$.^{11,13} Fits to this form are shown by solid lines in Figs. 4(e) and 4(f) and they give $\Gamma_1 = 0.7(1) \text{ meV}$ and $\Gamma_2 = 17(2)$ for $\text{Zn}_{0.95}\text{Cd}_{0.05}\text{Cr}_2\text{O}_4$ at $T = 40 \text{ K}$. The effects of doping become more pronounced close to the critical temperature. While the relaxation rate, $\Gamma_Q = 1.2(1) \text{ meV}$, remains finite for ZnCr_2O_4 at $T = 15 \text{ K}$, Cd doping broadens the relaxation rate distribution so that it extends from $\Gamma_1 = 0.08(1) \text{ meV}$ to $\Gamma_2 = 12(1) \text{ meV}$ for $\text{Zn}_{0.95}\text{Cd}_{0.05}\text{Cr}_2\text{O}_4$ close to T_f . Thus, the spin-glass-like transition can be associated with vanishing of the lower cutoff in the disorder broadened relaxation rate distribution.

We examine the spin dynamics through the freezing transition proper in Fig. 5. Frame (a) gives an overview of elastic and inelastic magnetic scattering versus temperature, while frame (b) shows constant energy cuts at the elastic position

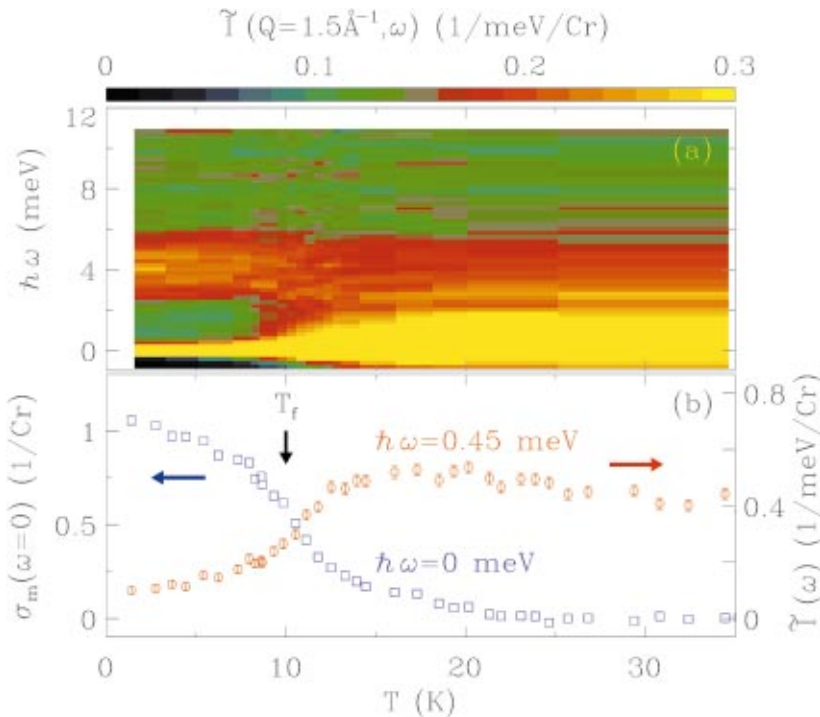


FIG. 5. (Color) (a) Color image of the temperature dependence of inelastic neutron scattering at $Q = 1.5 \text{ \AA}^{-1}$. (b) Blue squares show the temperature dependences of the elastic scattering for $Q = 1.5 \text{ \AA}^{-1}$. Red circles indicate the inelastic component of the intensity, integrated in the range of 0.3 meV to 0.6 meV . The black arrow indicates T_f as derived from bulk susceptibility data.

and for $\hbar\omega = (0.45 \pm 0.15)$ meV. The onset of diffuse elastic magnetic scattering for $T < 20$ K signals the development of short-range magnetic correlations on a time scale, $\tau > \hbar/\Delta E \approx 6.5$ ps set by the energy resolution of the instrument. Also marked in the figure is $T_f = 10$ K as determined by anomalies in dc susceptibility data. The discrepancy between the irreversibility temperature and the onset of elastic magnetic scattering is consistent with a precipitous softening of the magnetic fluctuation spectrum upon lowering T . As is common for spin glasses, this leads to anomalies when the lowest energy scale of the system falls below the characteristic energy scale of the measurement.¹² Unusual for a spin glass though, is the development of a pronounced inelastic peak at 4.5 meV below the freezing temperature. Both frames of Fig. 5 indicate that this peak develops out of quasi-elastic scattering that is pushed to higher energies in proportion to the strength of the elastic magnetic scattering cross section. In that regard it is similar to the resonance in pure ZnCr_2O_4 that develops abruptly at T_N just as the staggered magnetization in the long-range Néel ordered phase of that material.

Perhaps the most striking result of the experiment is the independence of the wave-vector dependence of the scattering from $\text{Zn}_{1-x}\text{Cd}_x\text{Cr}_2\text{O}_4$ on x and $T < \Theta_{CW}$. We have argued that this indicates that fluctuations in the paramagnetic phase can be described as fluctuations of spin-correlated nanoclusters. This interpretation also helps to explain the extreme sensitivity to bond disorder. Zn/Cd sites are tetrahedrally coordinated such that replacing a Zn cation by a Cd cation introduces distortions in the oxygen environments of four magnetic tetrahedra. The modified exchange interactions relieve frustration and enhance correlations between several spin-correlated nanoclusters, thus slowing their fluctuations. Consistent with experimental observations, the fluctuation spectrum and not the wave-vector dependence of the scattering is most strongly affected by such pinning. The random strain associated with Cd defects may also act to

preclude the coherent structural distortion that is associated with Néel order in ZnCr_2O_4 . Still mysterious is the fact that the 4.5 meV mode, albeit severely broadened in energy, seems to persist in the spin-glass-like state. The result indicates that the resonance mainly relies on there being a finite magnetization $\langle \mathbf{S} \rangle$ on individual lattice sites and less on the specific long-range periodicity of the static spin structure. It seems that the staggered magnetization acts as an effective field that causes spin-correlated nanoclusters to precess rather than fluctuate. The broadening of the resonance in Cd-doped samples would find its explanation in the broadened distribution of frozen magnetic environments in the spin-glass as compared to the Néel phase.

There are a number of nominally crystalline magnets with low-temperature quasistatic short-range-ordered spin configurations. These include the kagomé related systems $\text{SrCr}_9\text{pGa}_{12-9\text{p}}\text{O}_{19}$,¹⁴ the pyrochlore system $\text{Y}_2\text{Mo}_2\text{O}_7$,¹⁵ as well as the quantum spin chains SrCuO_2 ,¹⁶ and $\text{Ni}(\text{C}_5\text{D}_{14}\text{N}_2)_2\text{N}_3(\text{PF}_6)$.¹⁷ Our experiments on $\text{Zn}_{1-x}\text{Cd}_x\text{Cr}_2\text{O}_4$ probe ordered through disordered conditions and provide concrete evidence for extreme sensitivity to disorder in a near quantum critical spin system. We have shown that magnetism in this frustrated system distinguishes itself in that fluctuations involve spin-correlated nanoclusters. Such composite spin degrees of freedom characterize many systems that have glassy phases but no measurable disorder. We hypothesize that composite spin degrees of freedom promote hypersensitivity to disorder, as defects pin sizeable spin clusters rather than individual spins. A corollary is that the ultimate ground state of near quantum critical spin systems with composite spin degrees of freedom can only be ascertained in ultraclean limit samples.

Work on SPINS is based upon activities supported by the NSF through Grant No. DMR-9986442. The NSF supported work at Rutgers through Grant No. DMR-9802513 and work at JHU through Grant No. DMR-0074571.

¹C. Broholm *et al.*, in *Dynamical Properties of Unconventional Magnetic Systems*, Vol. 349 of *NATO Advanced Study Institute, Series E: Applied Sciences*, edited by A. T. Skjeltorp and D. Sherrington (Kluwer Academic, Boston, 1998), p. 77.

²A.P. Ramirez, in *Handbook of Magnetic Materials* (North-Holland, Amsterdam, 2001), Vol. 13, Chap. 4, p. 423.

³P. Chandra, P. Coleman, and I. Ritchey, *J. Phys. I* **3**, 591 (1993).

⁴M.J.P. Gingras *et al.*, *Phys. Rev. Lett.* **78**, 947 (1997).

⁵C.H. Booth *et al.*, *Phys. Rev. B* **62**, R755 (2000).

⁶A. Keren *et al.*, *Phys. Rev. Lett.* **87**, 177201 (2001).

⁷L. Bellier-Castella *et al.*, *Can. J. Phys.* **79**, 1365 (2001).

⁸S.-H. Lee *et al.*, *Phys. Rev. Lett.* **84**, 3718 (2000).

⁹D. Fiorani, S. Viticoli, J.L. Dormann, J.L. Tholence, and A.P. Muren, *Phys. Rev. B* **30**, 2776 (1984).

¹⁰S.M. Lovesey, *Theory of Thermal Neutron Scattering from Condensed Matter* (Clarendon Press, Oxford, 1984).

¹¹D.H. Reich, T.F. Rosenbaum, and G. Aeppli, *Phys. Rev. Lett.* **59**, 1969 (1987).

¹²J.A. Mydosh, *Spin Glasses* (Taylor & Francis, London, 1993).

¹³S.M. Hayden *et al.*, *Phys. Rev. Lett.* **66**, 821 (1991).

¹⁴S.-H. Lee *et al.*, *Europhys. Lett.* **35**, 127 (1996).

¹⁵J.S. Gardner *et al.*, *Phys. Rev. Lett.* **83**, 211 (1999).

¹⁶I.A. Zaliznyak *et al.*, *Phys. Rev. Lett.* **83**, 5370 (1999).

¹⁷Y. Chen *et al.*, *Phys. Rev. Lett.* **86**, 1618 (2001).